

# RSC Advances



This is an *Accepted Manuscript*, which has been through the Royal Society of Chemistry peer review process and has been accepted for publication.

*Accepted Manuscripts* are published online shortly after acceptance, before technical editing, formatting and proof reading. Using this free service, authors can make their results available to the community, in citable form, before we publish the edited article. This *Accepted Manuscript* will be replaced by the edited, formatted and paginated article as soon as this is available.

You can find more information about *Accepted Manuscripts* in the [Information for Authors](#).

Please note that technical editing may introduce minor changes to the text and/or graphics, which may alter content. The journal's standard [Terms & Conditions](#) and the [Ethical guidelines](#) still apply. In no event shall the Royal Society of Chemistry be held responsible for any errors or omissions in this *Accepted Manuscript* or any consequences arising from the use of any information it contains.



Journal Name

ARTICLE

# Self-assembled Structures of Polyhedral Gold Nanocrystals: Shape-directive Arrangement and Structure-dependence Plasmonic Enhanced Characteristics

Received 00th January 20xx,  
Accepted 00th January 20xx

DOI: 10.1039/x0xx00000x

www.rsc.org/

Yanting Liu,<sup>a</sup> Jun Zhou,<sup>\*a</sup> Lu Zhou,<sup>a</sup> Edwin Yue-Bun Pun,<sup>b</sup> Tao Jiang,<sup>a</sup>

Lucia Petti<sup>c</sup> and Pasquale Mormile<sup>c</sup>

Polyhedral gold nanocrystals (Au NCs) with quasi-spherical, octahedral and triangle-like morphologies were synthesized using hydrothermal method, and ordered packing structures were formed by water droplet evaporation-induced deposition. The self-assembled structures of the polyhedral Au NCs exhibit shape-directive arrangement during the building block orientation process, and the structure-dependence plasmonic characteristics of the self-assembled NCs were analysed numerically using finite element method (FEM). The surface-enhanced Raman scattering (SERS) spectra of the self-assembled structures were measured by choosing the 4-mercaptobenzoic acid as Raman reporter, using an excitation wavelength of 785 nm. Both the theoretical and experimental results show that the self-assembly structures of polyhedral Au NCs have high electric field enhancements and excellent SERS performances, in particular, the self-assembled structures of octahedron generate higher plasmonic enhancement efficiency compared to other close-packed configurations. The superior SERS behaviours can be explained based on the electromagnetic enhancement mechanism and the plasmonic antenna effect of the interstitial hot spots, confirming that the self-assembly structures of polyhedral Au NCs offer an alternate way in the design of plasmonic enhancement substrates, with potential applications in bio-sensing and medical detection.

## Introduction

Long-range ordered packing arrangements of inorganic nanocrystals (NCs) fabricated by spontaneous and assisted self-assembly method have attracted much attention in the nanofabrication field.<sup>1-4</sup> Various nanostructures with arbitrary geometric shapes have been developed into highly organized NCs assemblies.<sup>5-7</sup> Up to now, the drop casting approach induced by evaporation is the most common, simple and flexible method in arranging NCs into ordered

structures.<sup>8</sup> For example, densely pack and three-dimensional ordered structures of gold/silver NCs with spherical or non-spherical morphologies have been assembled through droplet evaporation method.<sup>4, 9-13</sup> In general, assembling NCs into ordered packing structures can be engineered by fulfilling three criteria: (i) the shapes and sizes of NCs as building blocks should be mono-dispersed and uniform; (ii) there is a passivation layer, for example, an appropriate surfactant; (iii) the drying process is controllable.<sup>14</sup> Also, there is a driving force that originate from the Vander Waals force or the electrostatic force in between the building blocks, or the chemical band force from surface-functionalized molecules during the assembly process.<sup>4,15</sup>

In the assembly of noble metal NCs, their elongated geometries are similar to periodic arrays and can induce a collective coupling effect of inter-particles, leading to special properties with potential applications in sensing, catalysis and medicine.<sup>16-19</sup> In particular, the localized surface plasmonic resonance (LSPR) characteristics are of great interest because the transfer and confinement of electromagnetic (EM) energy around the NCs can be further tuned and even amplified.<sup>20,21</sup> It is the plasmonic hot spot that arises from

<sup>a</sup>Institute of Photonics, Faculty of Science, Ningbo University, Ningbo 315211, China. Corresponding author: E-mail: zhoujun@nbu.edu.cn; Tel: +86-574-87600794; Fax: +86-574-87600744.

<sup>b</sup>Department of Electronic Engineering and State Key Laboratory of Millimeter Waves, City University of Hong Kong, Tat Chee Avenue, Kowloon, China

<sup>c</sup>Institute of Applied Sciences and Intelligent Systems "E. Caianiello" of CNR, Via Campi Flegrei, 34 - Comprensorio Olivetti, 80078 Pozzuoli (Napoli), Italy.

† Electronic Supplementary Information (ESI) available: additional SEM images of the assembled structures, the simulations of nanospheres array and the bowtie antennae structure.

the EM coupling between two adjacent NCs with a distance  $<10$  nm, resulting in an intense electric field enhancement.<sup>22-24</sup> Thus, the surface-enhanced Raman scattering (SERS) of well-ordered plasmonic hot spots in assembled structures of NCs is much higher than that of randomly spots on the surface of NCs.<sup>20, 23, 25</sup> The SERS signal of molecules which are located at plasmonic hot spots region around the surface of assembled structures can be amplified further to increase the sensitivity.<sup>11, 19</sup> Thus, the design and fabrication of plasmonic hot spots in assembled nanostructures is very important in order to obtain distinct SERS enhancement.<sup>26</sup>

The structure-dependence plasmonic enhancements of assembled noble metal NCs have been widely studied, and their SERS characteristics relating to the assembled architectures have been demonstrated.<sup>27-29</sup> For example, by adjusting the concentrations and the species of surface capping molecules, three dimension (3D) plasmonic arrays have been constructed by controllable self-assembly of Au nanorods, and the SERS performances exhibit structure-dependence for different arrangements of Au nanorods.<sup>12, 13, 18, 30</sup> Although closely-packing arrangements of noble metal NCs have been studied, attentions should be paid to the production of well-defined self-assembled structure of NCs with morphological diversity, because the packing and orientation behaviours of various assembled architectures will generate different and unique plasmonic hot spots which affect further the enhanced SERS properties.<sup>32-38</sup> Hence, it is important to study the assemblies of noble metal NCs with anisotropic geometric morphologies, tune and optimize their collective plasmonic properties for SERS-based applications.<sup>39-41</sup>

In this paper, drop casting method has been used to fabricate densely packed structures consisting of anisotropic polyhedral NCs building blocks. The structural characteristics of different ordered assemblies with variable-shaped Au NCs, including quasi-sphere, octahedron and triangle-analogue, are studied systematically. The assemblies are found to be strongly shape-dependent by their building block NCs, and the structure-dependence plasmonic enhanced behaviours of these assembled nanostructures have been analysed using the finite element method (FEM) in details. The assembled nanostructures show excellent response with an incident laser light wavelength of 785 nm in the Raman spectra measurement, due to the nanoantenna effect of the enhanced electric field of the assembled substrates.

## Experiments

### Chemicals

Hydrogen tetrachloroaurate (III) trihydrate ( $\text{HAuCl}_4 \cdot 3\text{H}_2\text{O}$ ) was purchased from Sigma Aldrich. Cetyltrimethylammonium bromide (CTAB) and trisodium citrate ( $\text{Na}_3\text{C}_6\text{H}_5\text{O}_7 \cdot 2\text{H}_2\text{O}$ ) were bought from Aladdin. 4-mercaptobenzoic acid (4-MBA) was obtained from J&K Scientific Co., Ltd. Si wafers with  $\langle 100 \rangle$  orientation were purchased from Sibranch Co., Ltd. Deionized water (Millipore Milli-Q grade) ( $18.2 \text{ M}\Omega \cdot \text{cm}^{-1}$  resistivity) was used for all solution preparation. All the chemicals are analytic grade and used as received. Glasswares were cleaned by aqua regia and rinsed with deionized water several times prior to the experiments.

### Preparation of polyhedral Au NCs and their self-assembled structures

Gold NCs with various geometric shapes were fabricated using procedures developed in our laboratory.<sup>42</sup> For typical synthesis of Au quasi-sphere, 10 ml of 15mM CTAB, 200  $\mu\text{l}$  of 0.01 M  $\text{HAuCl}_4$ , and 50  $\mu\text{l}$  of 100 M trisodium citrate aqueous solution were added sequentially and mixed in a 15 ml Teflon-lined stainless-steel autoclave, sealed and maintained at  $110^\circ\text{C}$  in an oven for 12 h. The autoclave was then cooled to room temperature naturally. The resulting Au NCs were collected by centrifugation at 8000 rpm for 20 min and washed with deionized water before another round of centrifugation to remove excess CTAB. Finally, the Au NCs were re-dispersed in deionized water for subsequent characterization. Similar procedures were used for the synthesis of octahedron (10.5 mM CTAB), truncated tetrahedron and bitetrahedron (described as triangle-analogue) NCs (4.5 mM CTAB), except that different concentrations of surfactant CTAB were used. The self-assembled structures of polyhedral Au NCs were prepared by drop casting 10  $\mu\text{L}$  volumes of the colloidal solution at a constant temperature ( $25^\circ\text{C}$ ) on silicon wafers.

### Preparation of 4-MBA-labelled polyhedral Au NCs substrates

The SERS performances of self-assembled polyhedral Au NCs were evaluated with 4-MBA Raman molecule. Firstly, the sample solutions were prepared by adding 20  $\mu\text{l}$  of 1 mM 4-MBA ethanol solutions into the as-purified 5ml of polyhedral Au NCs solutions under stirring, and the resultant solutions were agitated for 10 h. Next, the unbound 4MBA molecules in the solutions were removed by centrifuging at 8,000 rpm for 30 min and re-dispersed in 2 ml deionized water, and 4-MBA-labeled polyhedral Au NCs solutions were obtained. Finally, by drop casting 10  $\mu\text{L}$  volume of the colloidal solution on silicon wafers, self-assembled structures of polyhedral Au NCs on Si substrates were prepared and ready for the SERS measurements.

### Instruments

Scanning electron microscopy (SEM) (SU-70, Hitachi) instrument was utilized to characterize the morphologies of the nanostructures under an accelerating voltage of 5 kV. SERS signals were measured by a miniature Raman spectrometer (BWS415, B&W Tek Inc.) which is equipped with a 785-nm semiconductor laser as the excitation source. Raman spectrographs were recorded with a laser power of  $\sim 49.55$  mW and an accumulation time of 10 s. The scattered radiation of the substrate was collected by a 40 $\times$  objective lens with a NA of 0.65. The wavelength dispersion was performed using a 1200 lines/mm grating, and passed through a slit with 20  $\mu\text{m}$  width to a charge-coupled device (CCD) (2048 $\times$ 2048 pixels) detector. All the analyses were performed at room temperature.

### Calculation

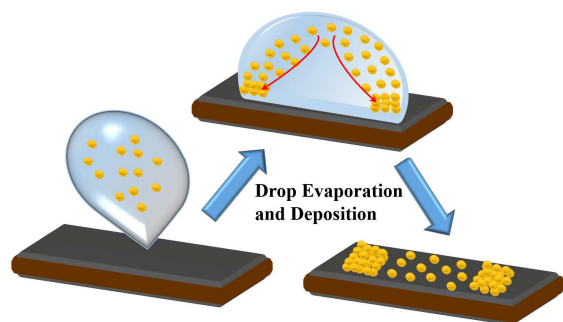
A series of numerical calculations were performed by using the incorporated RF module of the commercial software package (COMSOL Multiphysics 4.3). The electromagnetic properties of polyhedral Au NCs can be readily handled by the finite element

method (FEM) in an appropriate discrete spatial grid. In our calculations, the frequency dependent dielectric functions for gold are taken from the experimental bulk results of Johnson and Christy.<sup>43</sup> The surrounding medium is presumed to be air and the refractive index is 1.0. Based on the dimensions extracted from the SEM images of the self-assembled polyhedral Au NCs in our experiments, three-dimension nanostructure models were constructed to determine the electric field distributions in the actual assembled structures.

## Results and discussion

### Characterization of the self-assembly polyhedral Au NCs

As described in section 2.2, by adjusting the amounts of CTAB solution added to the reaction solutions, different geometric structures such as quasi-sphere, octahedron, and truncated tetrahedron and bitetrahedron can be obtained. The well-defined shapes and uniform sizes of these Au NCs have led to the observation of their long-range self-assembled arranged patterns with densely packed structures by evaporation-induced assembly.<sup>4</sup> In the drop casting process shown in Scheme 1, the Au NCs will reach critical concentration and deposit on the silicon wafer with evaporation of the water, and the assembly of Au NCs can be considered as an entropy increased procedure. After the solvent water was evaporated, the vast majority of NCs would usually stack into orderly arrangement structures closer to the edge of the droplet and formed a coffee ring region, due to the well-known coffee stain effect.<sup>8, 12, 44</sup> This is related to the capillary-induced flow, that is, Au NCs flow toward the edge of the droplet and the drop edge becomes pinned on the wafer during the drying process. The water evaporation from the edge is replenished by water from the interior, the capillary flow is outward from the center to the edge and carries all the NCs towards the edge, resulting in the deposition and concentration of NCs around the perimeter contact line of the droplet-wafer interface to form a ring like pattern.<sup>9-12</sup> In the coffee ring region, different self-assembled patterns are obtained by the geometric shapes of the polyhedral NCs building blocks in order that minimum surface energy of the assemble system is achieved.<sup>4, 14</sup>



**Scheme 1** The drop casting method of Au NCs

For the quasi-sphere Au NCs, they are spontaneously and closely packed into well-defined multilayers of face-centred-cubic (fcc) structures on silicon wafer, as shown in Fig. 1. Figure 1(a)-(c) show the different magnifications of the SEM images of the multilayer assembled structures, and Fig. 1(d) illustrates the packing mode of

the sphere building block. As shown in Fig. 1(c), there is an average inter-particle distance of  $\sim 5$  nm due to the existent of surface capping agent. It is well known that the surfactant CTAB molecules can form self-assembled micelles consisting of a bilayer of partially interdigitated CTAB molecules with 2-3 nm thickness, and leading to net positive charges on the NC surfaces.<sup>45</sup> This also provides the repulsive interactions among the NCs to prevent the random disordered aggregation during solvent evaporation.<sup>4</sup> Hence, the surfactant plays a crucial role in determining the formation of assembled structures.<sup>14</sup>

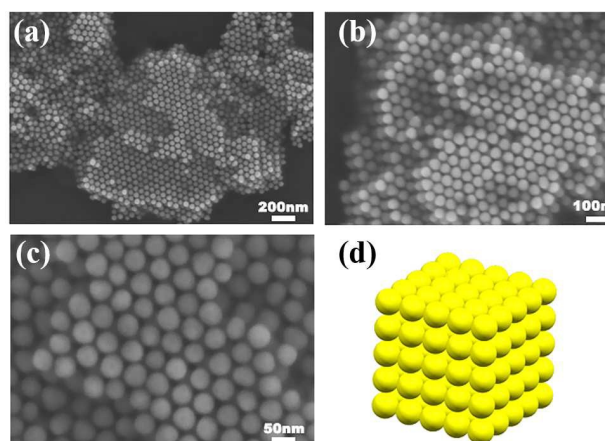


**Fig. 1** Different magnifications SEM images of multilayer assembled quasi-sphere Au NCs (a-c) and schematic of building blocks of the assembly structure (d)

The synthesized octahedral Au NCs appear to be highly monodisperse in sizes, and can be spontaneously assembled into two different types of well-ordered arrangements on the silicon wafer. As shown in Fig. 2 and Fig. 3, the representative SEM images of the self-assembled structures of the octahedral Au NCs exhibit a parallel closely-packed hexagonal array of the {111} facets and a row-by-row packed array misalignment-stack by the truncated {110} edges,

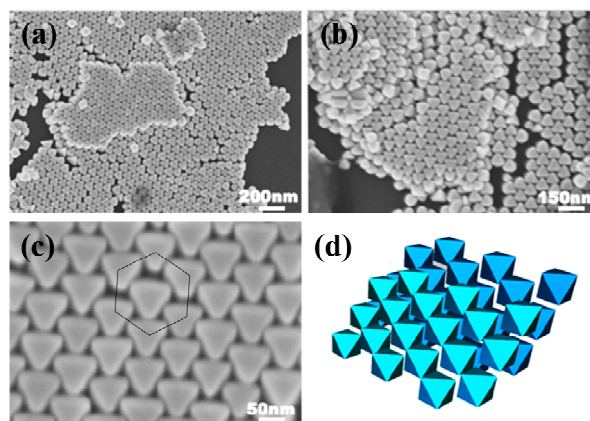


**Fig. 2** Different magnifications SEM images of self-assembled octahedral Au NCs (a)-(c) and schematic assembled structure of building blocks of type I (d). Inside (c) is a hexagonal arrangement.

and are known as types I and II, respectively. For type I arrangement, as shown in Fig. 2(a)-(c), it is a multi-layer structure and the

octahedron building blocks contact each other by their faces to form a closely-packed arrangement in each monolayer. Fig. 2(d) illustrate the schematic assembled structures of type I arrangement, and Fig. S1 shows the side view of the SEM images of the packed structures. The adjacent layers in the structures have a similar packing arrangement but an opposite and alternate packing orientation via complete or partial face-to-face contact, due to the fact that this

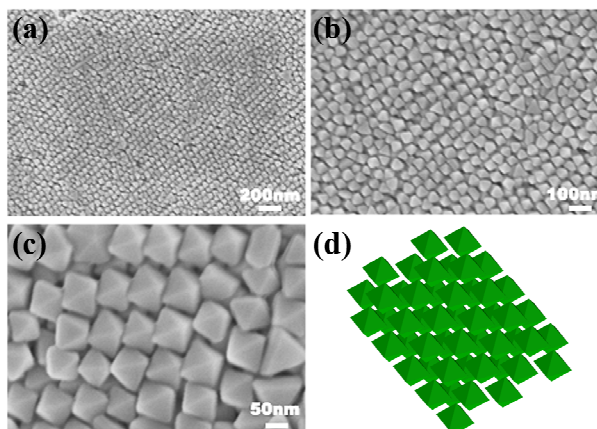


**Fig. 3** Different magnifications SEM images of self-assembled octahedral Au NCs (a)-(c) and schematic assembled structure of building blocks of type II (d).

deposition mode can minimize the free energy for such a layer-by-layer assembly.<sup>46</sup> For the type II arrangement, as shown in Fig. 3(a)-(c), the self-assembled structure is distinctly different from that of type I. Here the octahedrons form misalignment-stacked multi-layer structure by the slightly truncated corners contacting the underlying

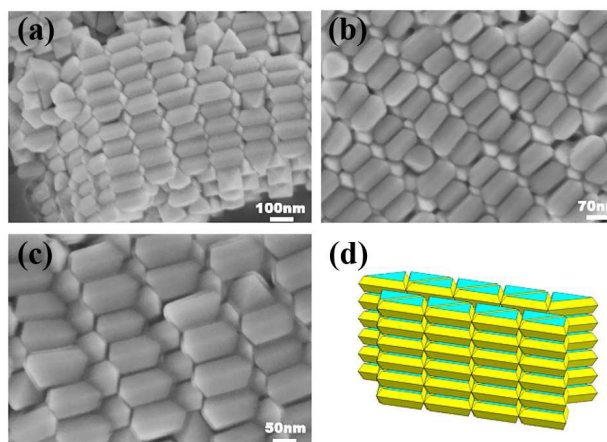


**Fig. 4** Different magnifications SEM images of multilayer assembled truncated bitetrahedral Au NCs on silicon substrates (a-c) and schematic image of assembly pattern of the building blocks (d)

substrate surface. This is also a stable packing arrangement, but requires the formation of a more extensive array of interlocking octahedrons to minimize the volume and the free energy. From Fig.

3(d), it can be seen that this packing structure is a regular array with a misaligned arrangement of adjacent octahedrons. The octahedron building blocks sacrifice some of the translation freedom on the horizontal plane in order to increase the orientation freedom along

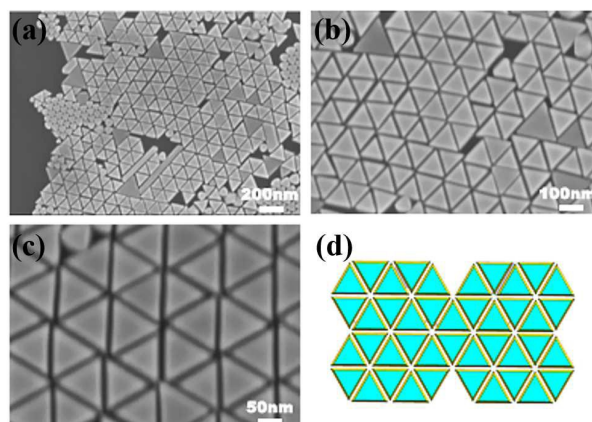


**Fig. 5** Different magnifications SEM images of self-assembled truncated tetrahedral Au NCs (a)-(c) and schematic assembled structure of building blocks (d).

the vertical direction by misalignment stacking of NCs. Comparing type I with type II from the view of structure stability, type I is easier to be formed by drop evaporation, and type II exist only as large arrays with increased colloid solution volume for stability reason.<sup>47</sup>

Furthermore, although the truncated tetrahedron and truncated bitetrahedron were obtained in the same procedure and they are twin products, the two triangle-analogues can be separately packed into different self-assembled structures, which are shown in Fig. 4 and Fig. 5, respectively. From Fig. 4(a)-(c), the truncated bitetrahedron NCs were interdigitated and formed into interlock self-assembled structures which are like fingers of folded hands. In Fig.4(d), the schematic shows the interlock closely-packed arrangement. The truncated bitetrahedron in adjacent upper and lower layer are face-to-face contact by the triangle (111) facets and then interlock with the truncated bitetrahedrons in other rows by the (110) facets. The face-to-face stack and interlock structure of the truncated bitetrahedrons is reconstructed in Fig.S2 for showing the 3D packing arrangement. On the other hand, the truncated tetrahedrons were packed into hexagonal arrangement, as shown in Fig. 5(a)-(c). It can be observed from Fig 5(c) that there is an interspatial distance of 3 nm between all of the repeat units in the hexagonal arrangement, and only 2D monolayer structure is spontaneously assembled during the drop evaporation of the Au truncated tetrahedron NCs solution. The inter-edge aggregated consequence of the truncated tetrahedron NCs is distinguished from the assembly of the truncated bitetrahedron. In another word, the difference between the assembled structures originated mainly from the different geometric shapes of NCs and the inter-NCs interactions.<sup>7</sup>

**Plasmonic enhancement and SERS performances of the self-assembled polyhedral Au NCs.**

Based on our previous work, the individual anisotropic polyhedral Au NCs have exhibited excellent plasmonic enhancement

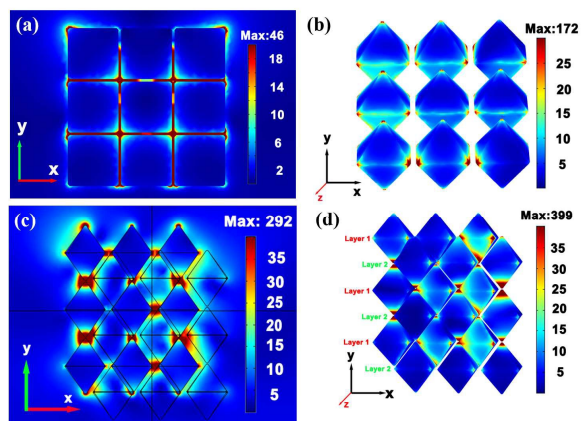


**Fig. 6** The electric field enhancement maps calculated for 3×3 monolayer Au octahedron (a) - (b) and the two-layer misalignment-stacked of self-assembled Au octahedron (c) - (d). The incident plane-wave with the 785nm wavelength and the polarization direction along x axis.

characteristics due to their strong LSPR coupling with exciting laser light.<sup>42</sup> Furthermore, the self-assemblies of polyhedral Au NCs can be regarded as periodic nanostructures of orderly closely-packed Au NCs. It can be expected that these self-assembled structures will build up a higher electric field enhancement due to the plasmonic hot spots in the assemblies of NCs. Therefore, 3D models were constructed for the packed arrangements of the different shapes of Au NCs to calculate numerically the distributions of the electric field intensities using the FEM.

To simplify the calculations in our simulations, only short-range ordered arrays are used in the modelling process. The electric field distributions of the monolayer and bilayer misalignment-stacked structures of Au octahedron arrays are simulated, and their cross-sectional views along x-y plane and 3D maps are shown in Fig. 6. It can be seen that the strongest enhancements of electric fields are located at the plasmonic hot spots, that is, the corners and edges of the octahedron building blocks, and can be attributed to the plasmonic antenna effect.<sup>13, 48-49</sup> By comparing the maximum values of electric field intensities in Fig. 6, the enhancement effect of the bilayer misalignment-stacked structures is higher than that of Au octahedron monolayer array. In fact, the bilayer misalignment-

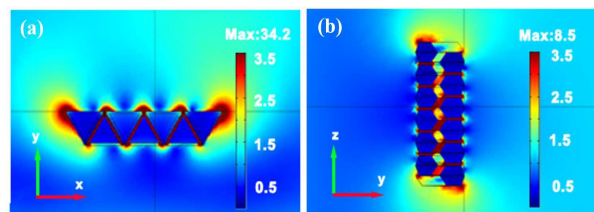


**Fig. 7** The electric field enhancement maps for two interlock arrays of truncated Au bitetrahedron along the x-y plane (a) and y-z plane (b), respectively.

stacked structures can produce more interstitial hot spots because there are more gaps in between the octahedron building blocks.<sup>50</sup>

On the other hand, the electric field intensity distributions of the self-assembled truncated Au tetrahedron and bitetrahedron have also been studied. Figure 7 shows the distributions of the electric field intensities of the interlock arrays composed of truncated Au bitetrahedrons under an excitation wavelength light of 785 nm and the polarization direction along the x axis. The maximums of the electric field distributions are at the positions of the corners, the edges and the faces of adjacent building blocks. As for assembled truncated Au tetrahedron, Fig. 8 shows that the stronger polarized light-induced electric fields are located around the inter-edges and the inter-corners. In Fig. 8(a), the enhanced electric fields of the hexagonally packed truncated Au tetrahedron NCs are located in the adjacent NCs due to the collective enhancement of plasmonic antenna effect of bowtie nanostructure (see in Fig. S3). Fig. 8(b) demonstrates stronger enhancement of the electric field intensities of the reproducible geometric nanostructure, and can be attributed to the superimposed effect of the repeat hexagonal units. In addition, the distribution of electric field intensity of the quasi-sphere array is similar to that of the sphere array (see Fig. S4). Comparing the maximum values of electric field intensity of the above four arrays, the enhanced electric field of the quasi-sphere array is much weaker than that of the other polyhedral assemble structures. It further confirms that the enhancement of the electric field of the assembled

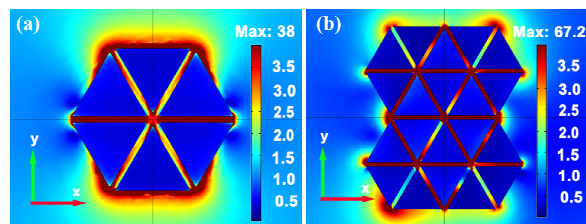


**Fig. 8** Electric field enhancement maps of truncated Au nanotetrahedron for a single hexagonal arrangement (a) and (b) four repeat unit of hexagonal arrangement

anisotropic nanostructures originate from the nano-antenna effect.

Based on the simulations of the self-assemble structures of Au NCs, the plasmonic properties of the assembled structures can be further determined by additional SERS investigations with incident laser light. The assembled nanostructures of the as-fabricated polyhedral Au NCs have a ~5 nm of gap in between the adjacent NCs, corresponding to a bilayer of the cationic surfactant (CTAB), and has been described as the optimal separation between particles for the generation of hot spots. It is the synergistic effect of the hot spots and antennae effect that contributes to the large enhancement of electrical field which is beneficial for SERS according to the electromagnetic enhancement mechanism.<sup>20, 21, 51</sup>

In our experiments, the SERS performances of these self-assembled polyhedral Au NCs were conducted with a 785-nm semiconductor laser as the excitation source. By using 4-MBA as the Raman reporter, the polyhedral NCs were first labeled with 4-MBA molecules and then dropped onto the silicon wafer for SERS detection. To achieve reliable measurement data, the SERS spectra of 10 random dots in the outer rim area of the coffee-ring region were recorded and shown in Fig.9. It can be observed that the SERS bands of the 4-MBA display fingerprint characteristics: two intense scattering peaks are located at ~1078 and 1590  $\text{cm}^{-1}$  which can be

ascribed to the two dominant Raman bands corresponding to the  $\nu$  (C-C) benzene ring-breathing modes. While other less intense modes, such as peak at  $718\text{ cm}^{-1}$  can be assigned to the out-of-plane  $13\beta(\text{CCC})$ ; peaks at  $847\text{ cm}^{-1}$  can be attributed the COO- bending mode ( $\delta(\text{COO-})$ );  $1152$  and  $1177\text{ cm}^{-1}$  originate from the bending mode ( $\nu(\text{C-H})$ ) on the benzene ring and a stretching mode at  $1430\text{ cm}^{-1}$  ( $\nu(\text{COO-})$ ), respectively. Due to the strong coupling between the transition dipole moment of benzene ring and local electric field, the  $\nu(\text{C-C})$  mode shows a higher intensity than that of the other modes.<sup>52-53</sup>

From the SERS spectra shown in Fig. 9, the assemblies of polyhedral Au NCs clearly show highly enhanced SERS activity as orderly packed structures, however, their SERS sensitivities and intensities are different. For illustration, the  $1078\text{ cm}^{-1}$  peak intensity of the 4-MBA of different assembled structures are shown in Fig. 9(d). The self-assembled structure of the octahedron Au NCs substrate has the strongest Raman signal, which can be ascribed to the closely-packed and ordered structure of the aligned octahedron building blocks. As described in the previous section, comparing with the assembled structures of quasi-sphere and triangle-analogue NCs, the octahedron Au NCs can easily form long-range ordered arrangements and well-defined profiles in the self-assemble process, so that stronger antenna effect and increase plasmonic hot spots are generated. It can be concluded that the influence of structure-dependence electric field enhancement is the main factor for the SERS enhancement, which is in agreement with the simulation results. For the self-assembled structures of triangular analogue NCs, the self-assembled truncated Au tetrahedron and bitetrahedron are on the same wafer and their SERS intensity is also better than that of the quasi-spheres NCs. It further confirms that the antenna effect plays a key role in determining the SERS efficiencies in self-assembled NCs. Also, there are two synergistic contributions that have to be considered in order to understand such enhancement, one is the number of hot spots in the orderly packed Au NCs structures, and the other is the structure-dependence antenna effect. Combining with the analysis of the plasmonic enhancement of each type of assembled structure, SERS activity depends mainly on the strong electric fields of the plasmonic hot spots that were distributed at sharp points with lightning rod effects. Therefore, it can be expecting that assembled polyhedral NCs can serve as superior SERS substrate for the detection of a wide variety of molecules.

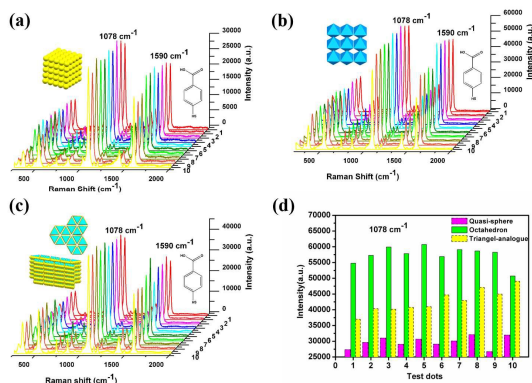


**Fig. 9** SERS spectra of 4-MBA at 10 random locations of self-assemble of quasi-sphere, octahedron and triangle-analogue Au NCs on silicon wafer.

## Conclusions

In this work, quasi-sphere, octahedral and triangle-analogue Au NCs have been used as building blocks to form various closely-packed arrangements on silicon wafers by drop casting method. It is found that the organized assembled structures are strongly shape-directive by the polyhedron Au NCs, suggesting that different NCs can adjust the contacts of building blocks during self-assembly process. Furthermore, the plasmonic properties and SERS performances of self-assembly structures of polyhedron Au NCs are also strongly shape-guided, or structure-dependence. The results are confirmed by the FEM simulations and SERS measurements for the self-assemble structures of polyhedron Au NCs. Among the different types of assembled structures of Au NC, the assembled structure of octahedral Au NCs exhibits superior SERS sensitivity compared with other shapes due to increase plasmonic hot spots and stronger antenna effect. The self-assembled procedure of diverse polyhedral structures by drop casting evaporation method allows the design of unique shape-directive assemble architectures, and the plasmonic properties can be tailored for ultrasensitive SERS detection of analytical targets relevant to medical and environmental sciences.

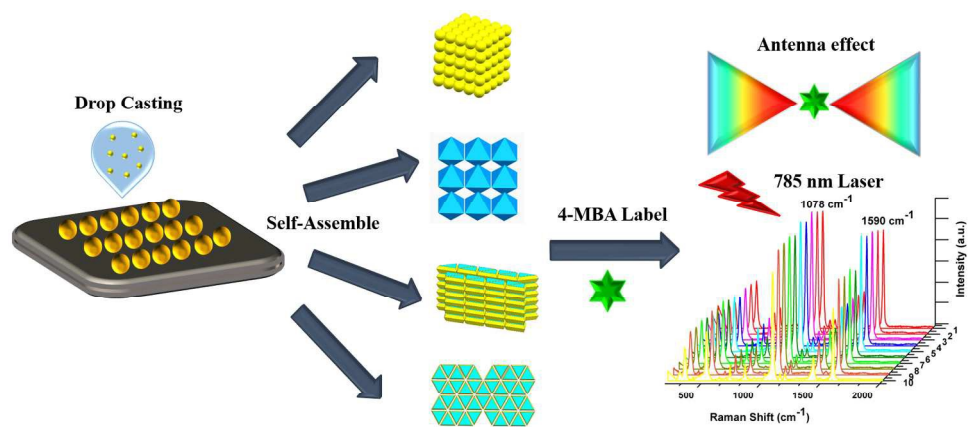
## Acknowledgements

This work was supported by the National Natural Science Foundation of China (Grant nos. 61320106014, 61275153, and 112064038), the European Regional Development Fund-FESR of POR Campania 2007-2013 - Call Innovation Window (Project title: Kit for Brucella Abortus e B. Melitensis nano-Biosensing Rapid detection- AMBRA), the Research Grants Council of Hong Kong under Project AOE/P-02/12, and the K. C. Wong Magna Foundation of Ningbo University, China.

## Notes and references

- <sup>a</sup> Institute of Photonics, Faculty of Science, Ningbo University, Ningbo 315211, China. Corresponding author: E-mail: zhoujun@nbu.edu.cn; Tel: +86-574-87600794; Fax: +86-574-87600744.
- <sup>b</sup> Department of Electronic Engineering and State Key Laboratory of Millimeter Waves, City University of Hong Kong, Tat Chee Avenue, Kowloon, China
- <sup>c</sup> Institute of Applied Sciences and Intelligent Systems "E. Caianiello" of CNR, Via Campi Flegrei, 34 - Comprensorio Olivetti, 80078 Pozzuoli (Napoli), Italy.
- † Electronic Supplementary Information (ESI) available: additional SEM images of the assembled structures, the simulations of nanospheres array and the bowtie antennae structure.
- 1 D. Vanmaekelbergh, *Nano Today*, 2011, **6**, 419-437.
- 2 F. A. Aldaye, A. L. Palmer and H. F. Sleiman, *Science*, 2008, **321**, 1795-1799.
- 3 J. Gong, G. Li and Z. Tang, *Nano Today*, 2012, **7**, 564-585.
- 4 C. J. Murphy, T. K. Sau, A. M. Gole, C. J. Orendorff, J. Gao, L. Gou, S. E. Hunyadi and T. Li, *J. Phys. Chem. B*, 2005, **109**, 13857-13870.
- 5 W. Li, K. Wang, P. Zhang, J. He, S. Xu, Y. Liao, J. Zhu, X. Xie and Z. Nie, *Small*, 2016, **12**, 499-505.
- 6 M. H. Huang and S. Thoka, *Nano Today*, 2015, **10**, 81-92.
- 7 Z. Quan and J. Fang, *Nano Today*, 2010, **5**, 390-411.
- 8 Z. Zhang and M. Lin, *J Mater. Chem. C*, 2014, **2**, 4545-4551.
- 9 P. Li, Y. Li, Z.-K. Zhou, S. Tang, X.-F. Yu, S. Xiao, Z. Wu, Q. Xiao, Y. Zhao, H. Wang and P. K. Chu, *Adv. Mater.*, 2016, **28**, 2511-2517.

- 10 C. Hamon, S. M. Novikov, L. Scarabelli, D. M. Solís, T. Altantzis, S. Bals, J. M. Taboada, F. Obelleiro and L. M. Liz-Marzán, *ACS Photonics*, 2015, **2**, 1482-1488.
- 11 A. Martín, C. Schopf, A. Pescaglini, J. J. Wang and D. Iacopino, *Langmuir*, 2014, **30**, 10206-10212.
- 12 K. C. Ng, I. B. Udagedara, I. D. Rukhlenko, Y. Chen, Y. Tang, M. Premaratne and W. Cheng, *ACS Nano*, 2012, **6**, 925-934.
- 13 R. A. Alvarez-Puebla, A. Agarwal, P. Manna, B. P. Khanal, P. Aldeanueva-Potel, E. Carbó-Argibay, N. Pazos-Pérez, L. Vigderman, E. R. Zubarev, N. A. Kotov and L. M. Liz-Marzán, *Proc. Natl. Acad. Sci. USA*, 2011, **108**, 8157-8161.
- 14 C. Wang, C. Siu, J. Zhang and J. Fang, *Nano Res.*, 2015, **8**, 2445-2466.
- 15 J. Wang, C. Sun, X. Liu, L. Xin and Y. Fang, *Colloid. Surf. A Physicochem. Eng. Asp.*, 2014, **455**, 104-110.
- 16 X. Li, J. Zhu and B. Wei, *Chem. Soc. Rev.*, 2016.
- 17 W. Ma, L. Xu, L. Wang, H. Kuang and C. Xu, *Biosens. Bioelectron.*, 2016, **79**, 220-236.
- 18 K. Thorkelsson, P. Bai and T. Xu, *Nano Today*, 2015, **10**, 48-66.
- 19 W. Li, L. Zhang, J. Zhou and H. Wu, *J. Mater. Chem. C*, 2015, **3**, 6479-6492.
- 20 Y. Xia and N. J. Halas, *MRS Bull.*, 2005, **30**, 338-348.
- 21 N. J. Halas, S. Lal, W.-S. Chang, S. Link and P. Nordlander, *Chem. Rev.*, 2011, **111**, 3913-3961.
- 22 C. Hamon and L. M. Liz-Marzán, *Chem.-Eur. J.*, 2015, **21**, 9956-9963.
- 23 M. Eguchi, D. Mitsui, H.-L. Wu, R. Sato and T. Teranishi, *Langmuir*, 2012, **28**, 9021-9026.
- 24 J. Henzie, S. C. Andrews, X. Y. Ling, Z. Li and P. Yang, *Proc. Natl. Acad. Sci. USA*, 2013, **110**, 6640-6645.
- 25 S. Gómez-Graña, C. Fernández-López, L. Polavarapu, J.-B. Salmon, J. Leng, I. Pastoriza-Santos and J. Pérez-Juste, *Chem. Mater.*, 2015, **27**, 8310-8317.
- 26 S. Dinda, V. Suresh, P. Thoniyot, A. Balčytis, S. Juodkazis and S. Krishnamoorthy, *ACS Appl. Mater. Interfaces*, 2015, **7**, 27661-27666.
- 27 Z. Zhu, H. Meng, W. Liu, X. Liu, J. Gong, X. Qiu, L. Jiang, D. Wang and Z. Tang, *Angew. Chem.*, 2011, **123**, 1631-1634.
- 28 M. J. Mulvihill, X. Y. Ling, J. Henzie and P. Yang, *J. Am. Chem. Soc.*, 2010, **132**, 268-274.
- 29 H. Ko, S. Singamaneni and V. V. Tsukruk, *Small*, 2008, **4**, 1576-1599.
- 30 S. Gómez-Graña, J. Pérez-Juste, R. A. Alvarez-Puebla, A. Guerrero-Martínez and L. M. Liz-Marzán, *Adv. Opt. Mater.*, 2013, **1**, 471-471.
- 31 C. Hamon, S. Novikov, L. Scarabelli, L. Basabe-Desmonts and L. M. Liz-Marzán, *ACS Nano*, 2014, **8**, 10694-10703.
- 32 Q. Shi, K. J. Si, D. Sikdar, L. W. Yap, M. Premaratne and W. Cheng, *ACS Nano*, 2016, **10**, 967-976.
- 33 C.-Y. Chiu, C.-K. Chen, C.-W. Chang, U. S. Jeng, C.-S. Tan, C.-W. Yang, L.-J. Chen, T.-J. Yen and M. H. Huang, *J. Am. Chem. Soc.*, 2015, **137**, 2265-2275.
- 34 C.-W. Yang, C.-Y. Chiu and M. H. Huang, *Chem. Mater.*, 2014, **26**, 4882-4888.
- 35 Y. Nakagawa, H. Kageyama, Y. Oaki and H. Imai, *J. Am. Chem. Soc.*, 2014, **136**, 3716-3719.
- 36 J. Henzie, M. Grünwald, A. Widmer-Cooper, P. L. Geissler and P. Yang, *Nat Mater*, 2012, **11**, 131-137.
- 37 H. Chan, A. Demortière, L. Vukovic, P. Král and C. Petit, *ACS Nano*, 2012, **6**, 4203-4213.
- 38 E. V. Shevchenko, D. V. Talapin, C. B. Murray and S. O'Brien, *J. Am. Chem. Soc.*, 2006, **128**, 3620-3637.
- 39 P. F. Damasceno, M. Engel and S. C. Glotzer, *Science*, 2012, **337**, 453-457.
- 40 C. Farcau, M. Potara, C. Leordean, S. Boca and S. Astilean, *Analyst*, 2013, **138**, 546-552.
- 41 S. Liu and Z. Tang, *J. Mater. Chem.*, 2010, **20**, 24-35.
- 42 Y. Liu, J. Zhou, X. Yuan, T. Jiang, L. Petti, L. Zhou and P. Mornile, *RSC Adv.*, 2015, **5**, 68668-68675.
- 43 P. B. Johnson and R. W. Christy, *Phys. Rev. B*, 1972, **6**, 4370-4379.
- 44 Y. Xie, S. Guo, C. Guo, M. He, D. Chen, Y. Ji, Z. Chen, X. Wu, Q. Liu and S. Xie, *Langmuir*, 2013, **29**, 6232-6241.
- 45 H. Wang, C. S. Levin and N. J. Halas, *J. Am. Chem. Soc.*, 2005, **127**, 14992-14993.
- 46 S. Xie, X. Zhou, X. Han, Q. Kuang, M. Jin, Y. Jiang, Z. Xie and L. Zheng, *J. Phys. Chem. C*, 2009, **113**, 19107-19111.
- 47 C.-C. Chang, H.-L. Wu, C.-H. Kuo and M. H. Huang, *Chem. Mater.*, 2008, **20**, 7570-7574.
- 48 M. s.-G. I. Santiago, M. Ryuji and K. Manabu, *J. Opt.*, 2015, **17**, 114001.
- 49 D. Radziuk and H. Moehwald, *Phys. Chem. Chem.*, 2015, **17**, 21072-21093.
- 50 Y. H. Lee, W. Shi, H. K. Lee, R. Jiang, I. Y. Phang, Y. Cui, L. Isa, Y. Yang, J. Wang, S. Li and X. Y. Ling, *Nat Commun*, 2015, **6**.
- 51 T. Honold, K. Volk, A. Rauh, J. P. S. Fitzgerald and M. Karg, *J. Mater. Chem. C*, 2015, **3**, 11449-11457.
- 52 A. Michota and J. Bukowska, *J. Raman Spectrosc.*, 2003, **34**, 21-25.
- 53 P. N. Sisco and C. J. Murphy, *J. Phys. Chem. A*, 2009, **113**, 3973-3978.



Self-assembly structures of different types of polyhedral nanocrystals through drop casting method and their plasmonic enhancement characteristics and SERS performances due to the nano-antenna effect

527x252mm (96 x 96 DPI)